Open-Access Full-Duplex Wireless in the ORBIT and COSMOS Testbeds

Manav Kohli*, Tingjun Chen*, Mahmood Baraani Dastjerdi*, Jackson Welles*, Ivan Seskar#, Harish Krishnaswamy*, Gil Zussman*
*Electrical Engineering, Columbia University, #WINLAB, Rutgers University
{mpk2138@, tingjun@ee., mb4038@, jw3350@, harish@ee., gil@ee.}columbia.edu, seskar@winlab.rutgers.edu

ABSTRACT

In order to support experimentation with full-duplex (FD) wireless, we recently integrated two generations of FD radios in the open-access ORBIT and COSMOS testbeds. First, we integrated a customized 1st generation (Gen-1) narrowband FD radio in the indoor ORBIT testbed. Then, we integrated two 2nd generation (Gen-2) wideband FD radios in the city-scale PAWR COSMOS testbed. Each integrated FD radio consists of an antenna, a customized RF self-interference (SI) canceller box, a USRP software-defined radio (SDR), and a remotely accessible compute node. The Gen-1/Gen-2 RF SI canceller box includes an RF canceller printed circuit board (PCB) which emulates a customized integrated circuit (IC) RF canceller implementation. The amplitude- and phase-based Gen-1 narrowband RF canceller achieves 40 dB RF SIC across 5 MHz. The Gen-2 wideband canceller is based on the technique of frequency-domain equalization (FDE) and achieves 50 dB RF SI cancellation (SIC) across 20 MHz. In this paper, we present the design and testbed integration of the two generations of FD radios. We then present example experiments that can be remotely run and modified by experimenters. Finally, we discuss future improvements and potential FD wireless experiments that can be supported by these open-access FD radios integrated in the COSMOS testbed.

CCS CONCEPTS

• **Networks → Network architectures**; *Wireless access networks*; *Network experimentation*; • **Hardware → Wireless devices**; Printed circuit boards.

WiNTECH'20, September 21, 2020, London, UK

ACM ISBN 978-1-4503-8082-9/20/09…$15.00
https://doi.org/10.1145/3411276.3412185

KEYWORDS

Full-duplex wireless; open-access wireless testbeds; wireless experimentation; frequency-domain equalization; self-interference cancellation; software-defined radios

ACM Reference Format:
Manav Kohli, Tingjun Chen, Mahmood Baraani Dastjerdi, Jackson Welles, Ivan Seskar, Harish Krishnaswamy, Gil Zussman. 2020. Open-Access Full-Duplex Wireless in the ORBIT and COSMOS Testbeds. In *14th International Workshop on Wireless Network Testbeds, Experimental evaluation & Characterization (WiNTECH'20), September 21, 2020, London, United Kingdom.* ACM, New York, NY, USA, 8 pages. https://doi.org/10.1145/3411276.3412185

1 INTRODUCTION

Due to its potential to double the data rate at the Physical (PHY) layer and to provide many other benefits at the higher layers of the networking stack, full-duplex (FD) wireless has drawn significant attention [1–4] as an enabler of next-generation wireless networks. One of the major challenges associated with enabling FD wireless is the extremely strong self-interference (SI) on top of the desired signal, requiring more than 90 dB of SI cancellation (SIC) across the antenna interface, and the RF/analog and digital domains.

Within the Columbia FlexICoN project [5], we focus on the design of and experimentation with FD radios and systems grounded in integrated circuit (IC) implementations, which are suitable for hand-held and form-factor-constrained devices [6]. In [7], we presented the 1st-generation (Gen-1) *narrowband* FD radio and an FD link, featuring 40 dB RF SIC across 5 MHz. This Gen-1 RF SI canceller emulates its RFIC counterpart presented in [8], whose modeling and analysis were presented in [9]. In [10], we developed a 2nd-generation (Gen-2) *wideband* FD radio which leverages the technique of frequency-domain equalization (FDE) to achieve over 50 dB RF SIC across 20 MHz, again emulating its RFIC counterpart presented in [11].

In order to allow the broader community to experiment with FD wireless, we integrated the two generations of FD radios in the open-access ORBIT [12] and COSMOS [13, 14] wireless testbeds, as shown in Fig 1. Since interfacing an RFIC canceller with a software-defined radio (SDR) presents

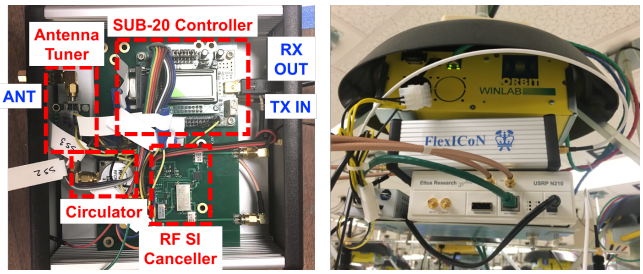

(a) **Gen-1 narrowband FD radio integrated in the ORBIT testbed.**

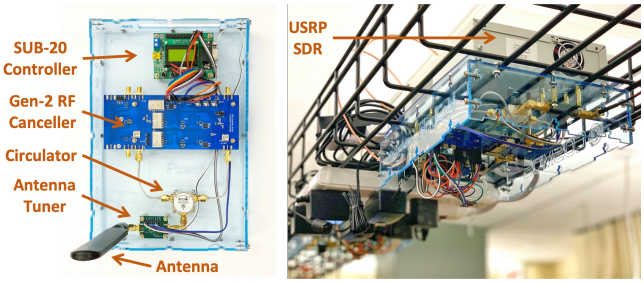

(b) **Gen-2 wideband FD radio integrated in the COSMOS testbed.**

Figure 1: **The two generations of integrated FD radios. Each FD radio consists of an antenna, a customized Gen-1/2 RF canceller box, a USRP SDR, and a remotely accessible compute node. Each RF canceller box contains an antenna tuner, a circulator, an RF canceller PCB, and a SUB-20 controller.**

numerous technical challenges, we implemented the RF cancellers on printed circuit boards (PCBs) to facilitate cross-layered experiments with an SDR platform. We first integrated an improved version of the Gen-1 RF canceller with a USRP N210 SDR in the ORBIT testbed [12]. We then followed a similar design and integrated two Gen-2 RF cancellers (an improved version of that presented in [10]) with USRP2 SDRs in the COSMOS testbed [13, 14].

In this paper, we first present the cross-layered (hardware and software) design and integration of a Gen-1 narrowband FD radio in the ORBIT testbed. We then present the design and integration of two Gen-2 FD wideband radios in the COSMOS testbed. Finally, we present two example experiments implemented in GNU Radio [15] that are available to experimenters: (i) real-time digital SIC, and (ii) measurements of the link-level packet reception ratio (PRR). These experiments show that our Gen-1/Gen-2 FD radios integrated in ORBIT/COSMOS can achieve over 80 dB of overall SIC across 5/12.5 MHz bandwidth, respectively.[1] These integrated remotely accessible FD radios and example experiments can also be further extended to more complicated networking scenarios.

[1]The performance is currently limited by USRP model and available compute resources, which are expected to be upgraded post-COVID-19 shutdown.

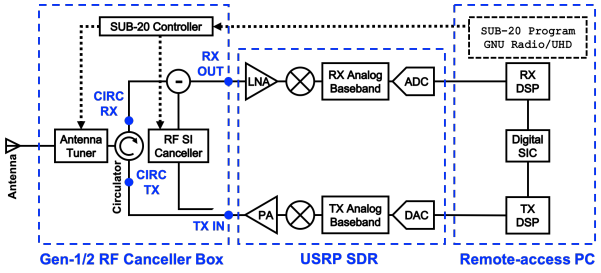

Figure 2: **Block diagram of the integrated FD radios with three main components: (i) a FlexICoN RF canceller box, (ii) a USRP software-defined radio (SDR), and (iii) a remotely accessible host PC on which experiments are run.**

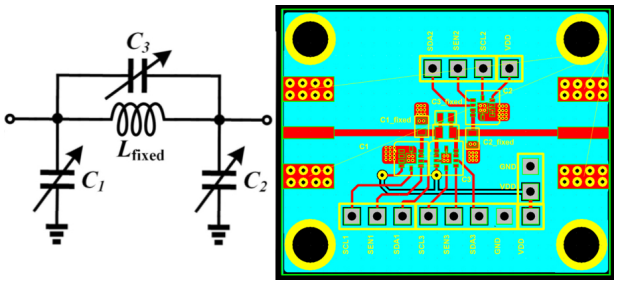

Figure 3: **Circuit diagram and PCB layout of the programmable antenna tuner as part of the Gen-1/Gen-2 RF canceller box.**

2 RELATED WORK

Extensive reviews of research in the area of FD wireless were presented in [1, 2], including various implementations of FD systems, and analysis of the influence of FD wireless at the higher layers of the networking stack. While [16–18] has involved a pair of Tx and Rx antennas to achieve Tx/Rx isolation at the antenna interface, we focus on FD radio designs using a shared antenna interface such as a circulator, which are more appropriate for single-antenna systems [3, 19]. In addition, existing circuit designs for RF/analog SIC often utilize a time-domain interpolation approach utilizing parallel delay lines with amplitude and phase control that are more suitable for discrete implementations on PCBs [3, 20]. We present two RF cancellers which utilize techniques suitable for achieving RF SIC in compact IC implementations.

The development of FD radios in previous research and associated investigation of effects on the higher layers took place in laboratory testbeds or in simulation [19, 21–23]. *To the best of our knowledge, this paper details the design and implementation of the first open-access, remotely accessible FD radios, together with open-source example experiments, that can be used by the community.*

3 DESIGN OF THE FLEXICON FD RADIOS

Fig. 2 shows the block diagram shared by both generations of FD radios. It consists of three main components: a Gen-1/2

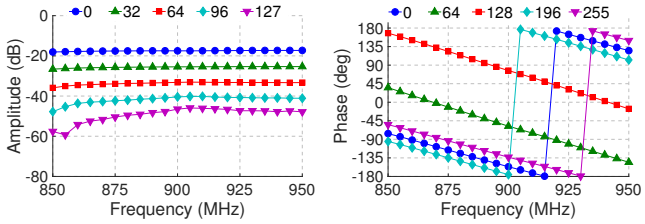

(a) (b)

Figure 4: **Measured amplitude and phase of the Gen-1 RF canceller PCB with varying (a) attenuation values, and (b) phase shift values.**

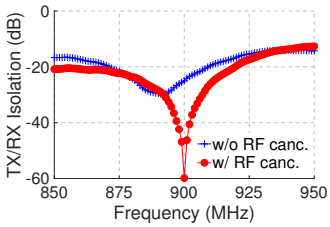

Figure 5: **Measured Tx/Rx isolation of the Gen-1 RF canceller box with and without turning on the RF canceller. The RF canceller box with the circulator and the RF canceller provides 40 dB RF SIC across 5 MHz bandwidth.**

RF canceller box, a USRP SDR, and a remotely accessible compute node. The SDRs used in ORBIT and COSMOS are the USRP N210 and USRP2, respectively, both of which have the same RF frontend.

Both the Gen-1 and Gen-2 RF canceller boxes share the same overall design as shown in Figs. 1 and 2. Each canceller box has four components: a circulator, an antenna tuner, a SUB-20 controller, and an RF canceller PCB which differs between Gen-1 and Gen-2. Below, we briefly discuss these components.

Coaxial Circulator. An RF-CI RFCR3204 coaxial circulator [24] is used, with operating frequency between 860–960 MHz.

Programmable Antenna Tuner. To achieve better matching between the antenna and the circulator, we also designed and implemented a programmable antenna tuner at around 900 MHz frequency. Fig. 3 shows the circuit diagram and PCB implementation of the antenna tuner. In particular, a π-network with lossless inductor (L) and digitally tunable capacitors (C_i) is used for impedance transformation. We use a fixed chip inductor with inductance $L_{\text{fixed}} = 5.1$ nH and Peregrine Semiconductor PE64909 5-bit digitally tunable capacitors for C_i ($i = 1, 2, 3$). By programming the capacitors with code values `CAPi` ($i = 1, 2, 3$), different antenna interface impedance matching can be achieved. The configuration ranges of the tunable capacitors are:

$$\texttt{CAPi} \in \{0, 1, \cdots, 15\}, \ \forall i = 1, 2, 3.$$

SUB-20 Controller. As Fig. 2 shows, a DIMAX SUB-20 multi-interface USB adapter [25] connected to the remote-access PC is used to program the tunable components on the RF canceller and antenna tuner through the serial peripheral interface (SPI). The SUB-20 SPI is configured to operate at the maximal SPI clock of 8 MHz. The SUB-20 control for both the Gen-1 and Gen-2 canceller PCBs is handled through a customized GNU Radio out-of-tree (OOT) module (see Section 6.1 for details).

RF Canceller PCB. In order to meet the USRP Rx front-end linearity and the analog-to-digital converter (ADC) dynamic range requirements, sufficient SIC in the RF domain is needed before digital SIC is performed. Therefore, the RF canceller PCB must provide up to 30 dB RF SIC in addition to the 20–25 dB provided by the circulator. The RF canceller taps a reference signal from the output of the power amplifier (PA) at the Tx side, and SIC is performed at the input of the low-noise amplifier (LNA) at the Rx side. The difference between the two generations of canceller boxes is the circuit design of the RF canceller PCB, as discussed in Sections 4.1 and 5.1.

4 GEN-1 FD RADIO

The Gen-1 FD radio is depicted in Fig. 1(a), including the components described in Section 3. In particular, the RF canceller PCB is a *narrowband* frequency-flat amplitude- and phase-based canceller, which is an improved version of that presented in [7]. In this section, we present the design and implementation of the Gen-1 FD radio, and its integration in the ORBIT testbed.

4.1 Gen-1 RF Canceller PCB

The amplitude- and phase-based RF canceller is implemented using discrete components on a PCB and is optimized around 900 MHz operating frequency.[2] The reference signal is tapped through a 6 dB Mini-Circuits ADC-6-13+ directional coupler whose amplitude and phase are subsequently adjusted before SIC is performed at the Rx.

For amplitude adjustment, a SKY12343-364LF 7-bit digital attenuator is used, and for phase adjustment, a Mini-Circuits passive SPHSA-152+ phase-shifter is used. The phase shifter is controlled by a TI-DAC081S101 8-bit digital-to-analog converter (DAC). The attenuator and DAC have a 3 V supply voltage, and the phase shifter has a reference voltage of 12 V. The attenuator and DAC are programmed through the SUB-20 controller over SPI. The available parameter configuration ranges for the attenuator `ATT` (ATTuation) and phase shifter `PS` (Phase Shift) are:

$$\texttt{ATT} \in \{0, 1, \cdots, 127\}, \ \texttt{PS} \in \{0, 1, \cdots, 255\}.$$

Fig. 4 shows the measured amplitude and phase responses of the RF canceller with varying `ATT` values (under fixed `PS` =

[2] In this implementation, we select 900 MHz operating frequency but this approach can be easily extended to other frequencies (e.g., 2.4/5 GHz).

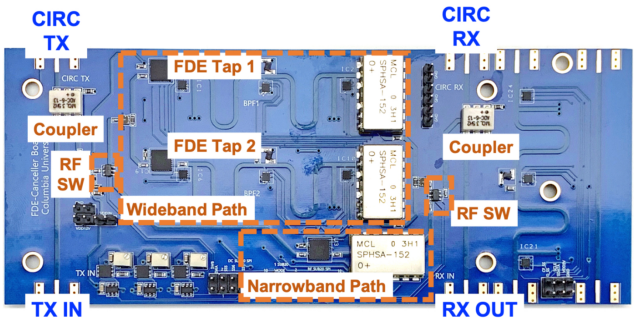

Figure 6: **The Gen-2 RF canceller PCB.**

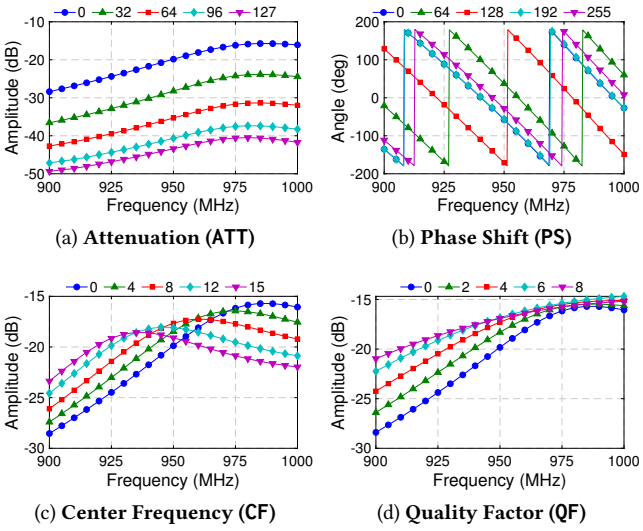

(a) **Attenuation (ATT)** (b) **Phase Shift (PS)**

(c) **Center Frequency (CF)** (d) **Quality Factor (QF)**

Figure 7: **Measured response of one FDE tap of the Gen-2 RF canceller with varying ATT, PS, CF, and QF values. The second FDE tap is turned off, and shares the same behavior.**

0) and with varying PS values (under fixed ATT = 0). The Gen-1 RF canceller has an amplitude tuning range between −48 dB and −17 dB, and a phase tuning range spanning the entire 360 deg range. Fig. 5 shows an example of the measured Tx/Rx isolation (measured between Tx IN and Rx OUT ports shown in Fig. 2), where 40 dB RF SIC is achieved across 5 MHz bandwidth.

4.2 Integration in the ORBIT Testbed

An ORBIT node equipped with the Gen-1 RF canceller box is depicted in Fig. 1(a). We use `node11-10` (the yellow box in Fig. 1(a)) in the ORBIT main `grid` with a USRP N210 SDR. In particular, the RF canceller box Tx IN/Rx OUT ports are connected to the USRP Tx/Rx ports respectively, and the RF canceller box ANT port is connected to an Apex II multi-band antenna. The USRP has a receiver noise floor of −86 dBm at 20 MHz bandwidth. We developed a node image

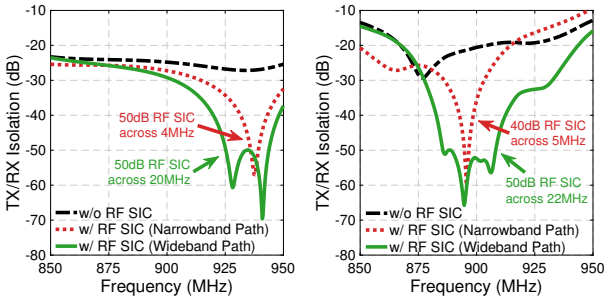

(a) **With 50 Ω termination.** (b) **With real antenna.**

Figure 8: **Measured RF SIC achieved by the Gen-2 RF canceller box with (i) the narrowband Gen-1 path (red line); (ii) the wideband FDE path (green line); and (iii) the canceller box switched off (black line). The circulator port is either (a) terminated by 50 Ω, or (b) connected to an antenna.**

(`flexicon-orbit-v3.ndz`) which contains the two example GNU Radio FD experiments (Section 6).

5 GEN-2 FD RADIO

The Gen-2 FD radio is depicted in Fig. 1(b). The Gen-2 RF canceller box includes an FDE-based RF canceller PCB which is an improved version of that described in [10].[3] This canceller PCB can achieve enhanced cancellation performance over a significantly wider bandwidth compared to the Gen-1 canceller PCB, and thus allows for experimentation with wider band signals. In this section, we present the design and implementation of the Gen-2 FD radio, and its integration in the COSMOS testbed.

5.1 Gen-2 RF Canceller PCB

The Gen-2 RF canceller illustrated in Fig. 6 is implemented using discrete components on a PCB and is optimized around a 900 MHz operating frequency.[4] The reference signal coupled from the Tx is first fed through an Analog Devices (ADI) HMC374 LNA before passing through an ADI HMC221B RF switch . This RF switch switches the reference signal between two paths: a Gen-1 narrowband path (identical to the Gen-1 RF canceller described in Section 4.1) and the wideband FDE path. In particular, the FDE path contains two parallel FDE taps, split and combined using Anaren PD0810J5050S2HF power dividers. Each FDE tap consists of a tunable bandpass filter (BPF) with amplitude and phase control.

Table 1 summarizes the tunable components on the Gen-2 canceller PCB. Each of the two paths contains an amplitude and phase control, identical to those on the Gen-1 canceller. Furthermore, each BPF is controlled by three tunable capacitors, which control the center frequency and quality factor of the BPF. For controlling the center frequency, we use

[3]The detailed design and evaluation of this canceller can be found in [10].
[4]As before, the design can be modified to other sub-6 GHz frequencies.

Table 1: **Summary of tunable components for the Gen-2 RF Canceller. $i \in \{0, 1\}$ represents the two FDE taps on the Gen-2 path.**

Scope	Control	Name	Tuning range
PCB	RF Switch	SW	$\{0, 1\}$
Gen-2 Path	Amplitude	ATTi	$\{0, \cdots, 127\}$
	Phase	PSi	$\{0, \cdots, 255\}$
	Center Frequency	CFi	$\{0, \cdots, 15\}$
	Quality Factor	QFi	$\{0, \cdots, 31\}$
Gen-1 Path	Amplitude	ATT2	$\{0, \cdots, 127\}$
	Phase	PS2	$\{0, \cdots, 255\}$

the Peregrine Semiconductor PE64102 4-bit digitally tunable capacitor with a tuning range of 1.88–14.0 pF. For controlling the quality factor, we use the Peregrine Semiconductor PE64909 5-bit digitally tunable capacitor with a tuning range of 0.6–2.35 pF. Together, these components provide a total of 2^{48} possible configurations for the Gen-2 path. The Gen-1 path contains an independent amplitude and phase control.

Fig. 7 shows the effect of varying each parameter on the frequency response of one individual FDE tap. In each case, only one parameter is varied, while the others are kept at their lowest values. Fig. 8 shows the achievable RF SIC of the wideband FDE path, where >50 dB RF SIC is achieved across 20 MHz bandwidth. This is 10 dB higher RF SIC achieved over 4× the bandwidth when compared to the Gen-1 path.

5.2 Integration in the COSMOS Testbed

The Gen-2 RF canceller box is integrated in the indoor COSMOS Sandbox 2 located at Columbia University. The antenna port is connected to a Larsen SPDA24700 LTE antenna [26], and the canceller box is connected to a USRP2 SDR. We integrate two Gen-2 radios, which form an FD link with 5 ft distance between antennas. Both Gen-2 FD radios are connected to the remotely accessible FD compute node: the SDR is connected over Ethernet and the SUB-20 controller over USB. The integration is shown in Fig. 1(b) and both identical Gen-2 FD radios are shown within the context of COSMOS Sandbox 2 in Fig. 9. The two USRP2s are synchronized over a MIMO cable.

The remotely accessible compute node is equipped with an Intel i7 8-core processor and 16 GB RAM, and runs Ubuntu 16.04, GNU Radio 3.7, and UHD 3.14 [15, 27]. This specification allows for running real-time experiments with a graphical user interface (GUI) above 10 MHz bandwidth. With the GUI disabled and use of the command line (terminal), the supported bandwidth can be increased to 25 MHz, which is the limit of the USRP2 SDRs.

6 REMOTE EXPERIMENTATION

Recall from Section 1 that the core feature of these integrated FD radios is that they can be remotely accessed by experimenters. The process for remotely accessing the FD radios

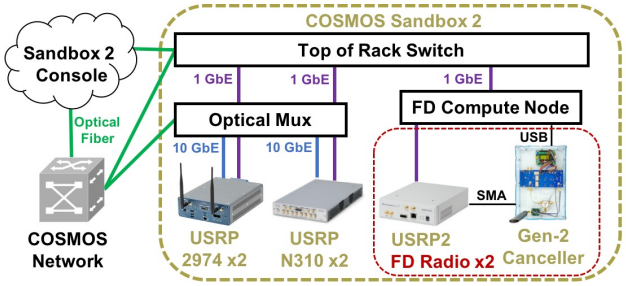

Figure 9: **COSMOS Sandbox 2 architecture, which includes (i) the remotely accessible console and two FD radios, each consisting of a USRP2 SDR and the Gen-2 canceller box, connected to the FD compute node, and (ii) other remotely accessible SDRs used for experimentation with various technologies.**

is the same for both ORBIT and COSMOS: the experimenter logs into the testbed console from their local machine using Secure Shell (SSH). X11 forwarding is used to enable the GNU Radio GUI on local machines. The tutorial with detailed instructions can be found at [28].

The developed example experiments run in *real-time*, where the experimenter can observe results visualized without offline processing. The example experiments employ an orthogonal frequency-division multiplexing (OFDM) PHY layer with variable bandwidth and modulation schemes. The example experiments, described below, can be used to benchmark several performance metrics of the ORBIT Gen-1 and COSMOS Gen-2 FD radios, including node-level SIC and link-level PRR.

6.1 Experiment 1: Node-Level Digital SIC

In this experiment, the experimenter can observe visualized real-time performance of one FD radio when transmitting OFDM packets. The following data is visualized: (i) the time domain Rx signal after RF SIC and after digital SIC, (ii) the power spectrum of the Rx signal after RF SIC and after digital SIC, (iii) the digital SIC filter taps, and (iv) the constellations after RF SIC and after digital SIC.

As mentioned in Section 5.2, the provided GNU Radio experiments operate in real-time. This is accomplished by the use of customized C++ out-of-tree (OOT) blocks, which are optimized for real-time performance. The implemented OOT blocks are available at [29] and described below:

SUB-20 Control. A core part of this experiment is the ability of the experimenter to manually configure the canceller PCB to achieve different RF SIC profiles. The experimenter has access to a GUI with controls that allow the full range of input described in Table 1. The numerical values set by these GUI controls are input to the SUB-20 control OOT block, which then uses the SUB-20 application programming interface (API) [25] to generate the appropriate SPI frames to be transmitted to the RF canceller PCB. For the Gen-1 and

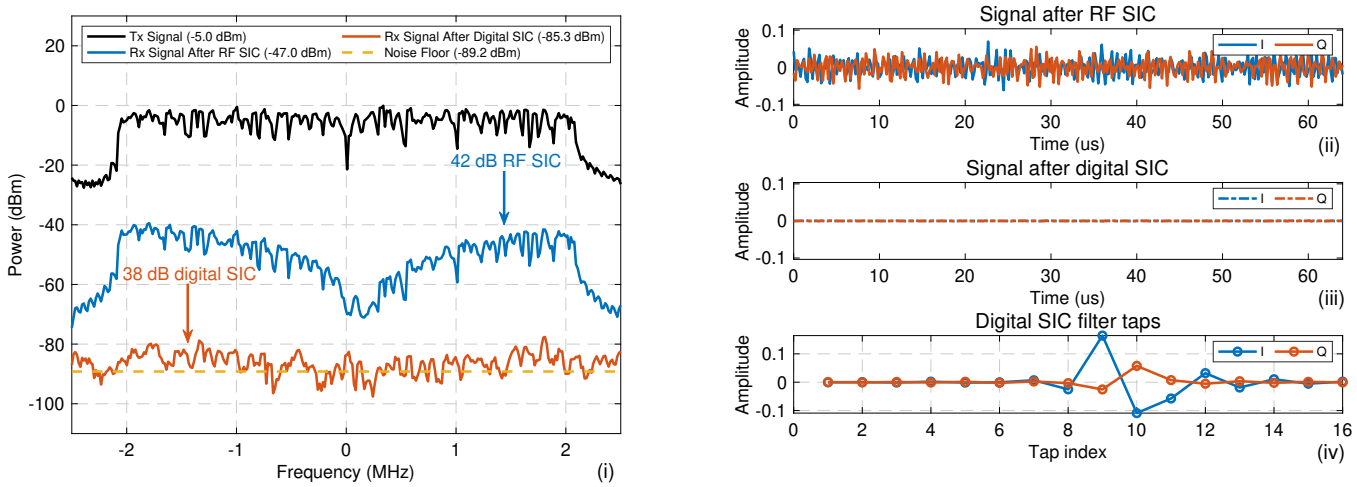

(a) **Gen-1 FD radio at 909 MHz carrier frequency with 5 MHz bandwidth.**

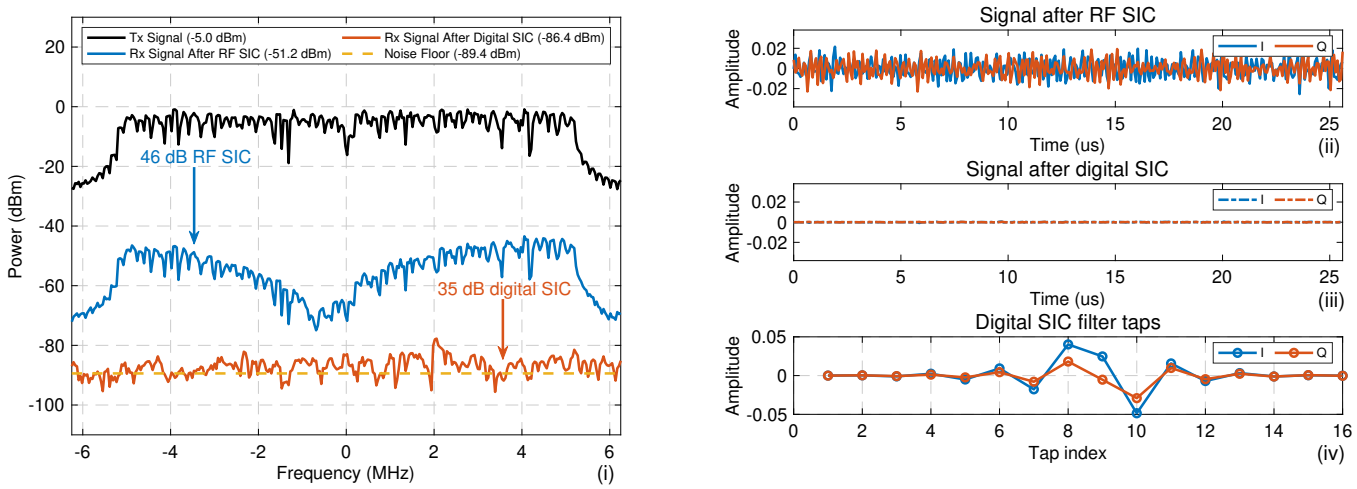

(b) **Gen-2 FD radio at 915 MHz carrier frequency with 12.5 MHz bandwidth.**

Figure 10: **Node-level self-interference cancellation (SIC) performance for (a) the ORBIT Gen-1 FD radio, and (b) the COSMOS Gen-2 FD radio. Data shown are (i) power spectrum of the received signal after SIC in the RF and digital domains; (ii), (iii) time domain signals after RF and after digital SIC; (iv) digital SIC filter taps. The average Tx power is −5 dBm, and the receiver noise floor is −89 dBm.**

Gen-2 RF cancellers, a total of 7 and 23 bytes, respectively, are sent over SPI to program the canceller PCB and antenna tuner. With an 8 MHz SPI clock, one configuration of the Gen-1 and Gen-2 canceller PCBs takes 7 μs and 23 μs, respectively. Therefore, different RF SIC profiles may be visualized in real time.

Digital SIC. Digital SIC is performed on the packet-level using a least-squares algorithm to estimate the SI channel in the time domain with additional pilot OFDM symbols. The OOT block performs both the least-squares SI channel estimation and digital SIC with the following computation: $\mathbf{r}_{\text{Rx}} = \mathbf{y}_{\text{Rx}} - \mathbf{A}\hat{\mathbf{h}}$. Here, $\mathbf{r}_{\text{Rx}}$ is the residual SI after RF and digital SIC, $\mathbf{y}_{\text{Rx}}$ is the signal after RF SIC, $\mathbf{A}$ is the the Toeplitz matrix constructed from the transmitted signal, and $\hat{\mathbf{h}}$ is the estimated SI channel (i.e., the digital SIC filter taps).

Packet Encapsulation. The implemented digital SIC algorithm requires additional pilot symbols prepended to every packet. We implemented a customized OOT block to prepend these symbols, and to add zero padding between packets.

SIC Performance. Fig. 10 shows the node-level SIC performance of the Gen-1 narrowband FD radio in ORBIT and the Gen-2 wideband FD radio integrated in COSMOS. By configuring the RF cancellers appropriately, the Gen-1 FD radio can achieve 35–40 dB RF SIC across 3–5 MHz, and the Gen-2 FD radio can achieve 45–50 dB RF SIC across 15–20 MHz. In both cases, the RF SIC is followed by 35–40 dB of digital SIC for around 80 dB overall SIC. We will replace the USRP2 with

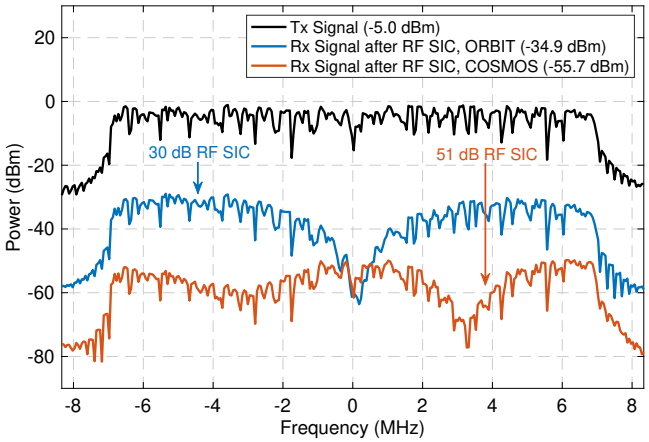

Figure 11: **RF SIC achieved over 16.6 MHz for the Gen-1 and Gen-2 FD radios. The Gen-2 wideband FD radio can achieve a greater RF SIC over a wider signal bandwidth.**

the higher performance USRP 2974, which will improve the amount of achievable digital SIC.

For the integrated Gen-1 and Gen-2 FD radios, the RF SIC performance alone is illustrated over a wider bandwidth in Fig. 11, which clearly shows the Gen-1/Gen-2 narrowband/wideband performances. Across the 16.6 MHz bandwidth shown in the figure, the Gen-1 FD radio can achieve 30 dB RF SIC, whereas the Gen-2 FD radio can achieve 50 dB RF SIC.

6.2 Experiment 2: Link-Level FD Packet Reception Ratio (PRR)

The experimenter can also use the two Gen-2 FD radios to perform link-level experimentation. In this experiment, link PRR as a function of the signal-to-noise ratio (SNR) is measured while the two Gen-2 FD radios operate in half-duplex (HD) or FD mode. To achieve a successful FD link, the experimenter can configure each FD node via the methods described in Section 6.1 to achieve the desired SIC across the RF and digital domains. The Tx power of the FD radios is swept during the experiment. For each Tx power value, the FD radios transmit 1,024 OFDM packets. Three different modulation schemes are used without any channel coding: binary phase shift keying (BPSK), quadrature phase shift keying (QPSK), and 8-phase shift keying (8PSK).

We consider two performance metrics. The first is the *HD or FD link SNR*, which is measured as the ratio between the average Rx signal power level (across all 1,024 packets) and the Rx noise floor when the link operates in HD or FD mode. The second metric is the *HD or FD link PRR*, which is calculated for each FD radio as the percentage of the 1,024 transmitted packets that are successfully received and decoded. Fig. 12 plots the measured HD and FD link PRR as a

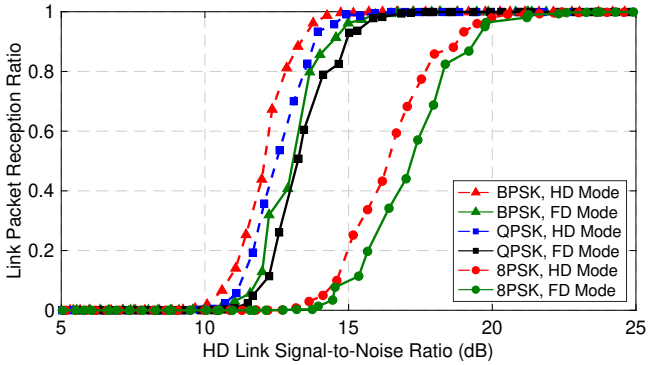

Figure 12: **HD and FD link packet reception ratio (PRR) for BPSK-, QPSK-, and 8PSK-modulated, uncoded OFDM packets with varying HD link SNR.**

function of the HD link SNR. The results show that with sufficient link SNR values, the Gen-2 FD radio can achieve a PRR of 1. This corresponds to a link-level FD rate gain of exactly 2×. With insufficient link SNR values, there is a reduction in PRR of 15% on average, which corresponds to an average link-level FD rate gain of 1.7×. The lower PRR values are a result of degradation in link SNR when the radios operate in FD mode, due to imperfect SIC.

7 CONCLUSION

In this paper, we presented our cross-layered (hardware and software) design and implementation of the first open-access, remotely accessible FD radios integrated in the ORBIT and COSMOS wireless testbeds. The presented example experiments along with the tutorial can be expanded to different network scenarios. Therefore, the integrated FD radios and example experiments can facilitate further hands-on research in FD wireless

When physical access to the COSMOS testbed is restored, we plan to make several improvements to the integrated FD radios. In particular, we will replace the USRP2s with USRP 2974s, which have better performance that includes supporting a higher signal bandwidth. This will facilitate the use of more complex OFDM PHY layer waveforms [30]. We will also utilize the servers in COSMOS Sandbox 2, which provide heterogenous computing resources, including CPUs, GPUs, and FPGAs.

We anticipate that these improvements will allow for more complex experiments, including at the medium access control (MAC) layer [31]. Integration with the Sandbox 2 servers will also allow for experimentation across the radio, compute, and optical domains [32].

ACKNOWLEDGMENTS

This work was supported in part by NSF grants ECCS-1547406 and CNS-1827923, NSF-BSF grant CNS-1910757,

DARPA RF-FPGA and SPAR programs, and a Facebook Fellowship. We thank Jelena Diakonikolas, Guy Farkash, Jakub Kolodziejski, Prasanthi Maddala, Jonathan Ostrometzky, Michael Sherman, and Jin Zhou for their contributions to various aspects of the project.

REFERENCES

[1] Ashutosh Sabharwal, Philip Schniter, Dongning Guo, Daniel W Bliss, Sampath Rangarajan, and Risto Wichman. In-band full-duplex wireless: Challenges and opportunities. *IEEE J. Sel. Areas Commun.*, 32(9):1637–1652, 2014.

[2] Kenneth E. Kolodziej, Bradley T. Perry, and Jeffrey S. Herd. In-band full-duplex technology: Techniques and systems survey. *IEEE Trans. Microw. Theory Techn.*, 67(7):3025–3041, 2019.

[3] Dinesh Bharadia, Emily McMilin, and Sachin Katti. Full duplex radios. In *Proc. ACM SIGCOMM'13*, 2013.

[4] Liang Zhang and Nirwan Ansari. A framework for 5G networks with in-band full-duplex enabled drone-mounted base-stations. *IEEE Wireless Commun.*, 26(5):121–127, 2019.

[5] The Columbia FlexICoN project. https://flexicon.ee.columbia.edu/.

[6] Jin Zhou, Negar Reiskarimian, Jelena Diakonikolas, Tolga Dinc, Tingjun Chen, Gil Zussman, and Harish Krishnaswamy. Integrated full duplex radios. *IEEE Commun. Mag.*, 55(4):142–151, 2017.

[7] Tingjun Chen, Jin Zhou, Nicole Grimwood, Rel Fogel, Jelena Marašević, Harish Krishnaswamy, and Gil Zussman. Demo: Full-duplex wireless based on a small-form-factor analog self-interference canceller. In *Proc. ACM MobiHoc'16*, 2016.

[8] Jin Zhou, Anandaroop Chakrabarti, Peter Kinget, and Harish Krishnaswamy. Low-Noise Active Cancellation of Transmitter Leakage and Transmitter Noise in Broadband Wireless Receivers for FDD/Co-Existence. *IEEE J. Solid-State Circuits*, 49(12):1–17, 2014.

[9] Jelena Marasevic, Jin Zhou, Harish Krishnaswamy, Yuan Zhong, and Gil Zussman. Resource allocation and rate gains in practical full-duplex systems. *IEEE/ACM Trans. Netw.*, 25(1):292–305, 2017.

[10] Tingjun Chen, Mahmood Baraani Dastjerdi, Jin Zhou, Harish Krishnaswamy, and Gil Zussman. Wideband full-duplex wireless via frequency-domain equalization: Design and experimentation. In *Proc. ACM MobiCom'19*, 2019.

[11] Jin Zhou, Tsung-Hao Chuang, Tolga Dinc, and Harish Krishnaswamy. Integrated Wideband Self-Interference Cancellation in the RF Domain for FDD and Full-Duplex Wireless. *IEEE J. Solid-State Circuits*, 50(12):3015–3031, 2015.

[12] Open-access research testbed for next-generation wireless networks (ORBIT). https://www.orbit-lab.org/.

[13] Dipankar Raychaudhuri, Ivan Seskar, Gil Zussman, Thanasis Korakis, Dan Kilper, Tingjun Chen, Jakub Kolodziejski, Michael Sherman, Zoran Kostic, Xiaoxiong Gu, Harish Krishnaswamy, Sumit Maheshwari, Panagiotis Skrimponis, and Craig Gutterman. Challenge: COSMOS: A City-Scale Programmable Testbed for Experimentation with Advanced Wireless. In *Proc. ACM MobiCom'20*, 2020.

[14] Cloud Enhanced Open Software Defined Mobile Wireless Testbed for City-Scale Deployment (COSMOS). https://cosmos-lab.org/, 2020.

[15] GNU Radio. http://gnuradio.org/.

[16] Jung Il Choi, Mayank Jain, Kannan Srinivasan, Phil Levis, and Sachin Katti. Achieving single channel, full duplex wireless communication. In *Proc. ACM MobiCom'10*, 2010.

[17] Bozidar Radunovic, Dinan Gunawardena, Peter Key, Alexandre Proutiere, Nikhil Singh, Vlad Balan, and Gerald Dejean. Rethinking indoor wireless mesh design: Low power, low frequency, full-duplex. In *Proc. IEEE WIMESH'10*, 2010.

[18] Mayank Jain, Jung Il Choi, Taemin Kim, Dinesh Bharadia, Siddharth Seth, Kannan Srinivasan, Philip Levis, Sachin Katti, and Prasun Sinha. Practical, Real-Time, Full Duplex Wireless. In *Proc. ACM MobiCom'11*, 2011.

[19] MinKeun Chung, Min Soo Sim, Jaeweon Kim, Dong Ku Kim, and Chan-Byoung Chae. Prototyping real-time full duplex radios. *IEEE Commun. Mag.*, 53(9):56–63, 2015.

[20] Dani Korpi, Joose Tamminen, Matias Turunen, Timo Huusari, Yang-Seok Choi, Lauri Anttila, Shilpa Talwar, and Mikko Valkama. Full-duplex mobile device: Pushing the limits. *IEEE Commun, Mag.*, 54(9):80–87, 2016.

[21] Ehsan Aryafar and Alireza Keshavarz-Haddad. FD2: A directional full duplex communication system for indoor wireless networks. In *Proc. IEEE INFOCOM'15*, 2015.

[22] Kai-Cheng Hsu, Kate Ching-Ju Lin, and Hung-Yu Wei. Inter-client interference cancellation for full-duplex networks. In *Proc. IEEE INFOCOM'17*, 2017.

[23] Shih-Ying Chen, Ting-Feng Huang, Kate Ching-Ju Lin, Y-W Peter Hong, and Ashutosh Sabharwal. Probabilistic medium access control for full-duplex networks with half-duplex clients. *IEEE Trans. Wireless Commun.*, 16(4):2627–2640, 2017.

[24] RF-CI SMA-F Circulator Model RFCR3204, mechanical drawing and data sheet. http://www.rf-ci.com/wp-content/themes/rfci/pdf/sma-connector-thin-circulator-communication/CR3204-OSrA.pdf. Accessed on 06/20/2020.

[25] DIMAX SUB-20 user manual. https://www.xdimax.com/sub20/doc/sub20-man.pdf. Accessed on 05/15/2019.

[26] Pulse larsen spda24700/2700 swivel blade antenna. https://www.wpsantennas.com/SPDA247002700-Swivel-Blade-omnidirection.aspx.

[27] USRP Hardware Driver (UHD) software. https://github.com/EttusResearch/uhd. Accessed on 07/01/2020.

[28] Tutorial: Full-duplex wireless in the ORBIT and COSMOS testbeds. https://wiki.cosmos-lab.org/wiki/Tutorials/Wireless/FullDuplex, 2020.

[29] The Columbia FlexICoN project: Instructions and Code. https://github.com/Wimnet/flexicon_orbit, 2020.

[30] Bastian Bloessl, Michele Segata, Christoph Sommer, and Falko Dressler. An IEEE 802.11a/g/p OFDM Receiver for GNU Radio. In *Proc. SRIF'13*, Aug. 2013.

[31] Tingjun Chen, Jelena Diakonikolas, Javad Ghaderi, and Gil Zussman. Hybrid Scheduling in Heterogeneous Half-and Full-Duplex Wireless Networks. *IEEE/ACM Trans. Netw.*, 28(2):764–777, Apr. 2020.

[32] Artur Minakhmetov, Craig Gutterman, Tingjun Chen, Cedric Ware, Luigi Iannone, Dan Kilper, and Gil Zussman. Experiments on cloud-RAN wireless handover using optical switching in a dense urban testbed. In *Proc. OSA OFC'20*, 2020.